AGU100 ADVANCING EARTH AND SPACE SCIENCE

Geophysical Research Letters

RESEARCH LETTER
10.1029/2018GL077607

Key Points:
- Fiber optic sensing with Rayleigh backscattering produces a clear-cut profile of the strain changes along a borehole in a landslide
- Visualization of an unknown deformation of the mudstone layer below a slip plane has been achieved
- Deeper sections of the landslide appear to have been gradually activated by heavy rainfalls

Supporting Information:
- Supporting Information S1

Correspondence to:
T. Kogure,
kogure@riko.shimane-u.ac.jp

Citation:
Kogure, T., & Okuda, Y. (2018). Monitoring the vertical distribution of rainfall-induced strain changes in a landslide measured by distributed fiber optic sensing with Rayleigh backscattering. *Geophysical Research Letters*, *45*, 4033–4040. https://doi.org/10.1029/2018GL077607

Received 18 FEB 2018
Accepted 5 APR 2018
Accepted article online 19 APR 2018
Published online 4 MAY 2018

Monitoring the Vertical Distribution of Rainfall-Induced Strain Changes in a Landslide Measured by Distributed Fiber Optic Sensing With Rayleigh Backscattering

Tetsuya Kogure[1] **and Yudai Okuda**[1]

[1]Department of Geoscience, Interdisciplinary Graduate School of Science and Engineering, Shimane University, Matsue, Japan

Abstract Distributed fiber optic sensing with Rayleigh backscattering, which has been recognized as a novel technique for measuring differences in temperature or strain, was adopted in a borehole to a depth of 16 m in an actual landslide to detect a vertical profile of strain changes. Strain changes were measured every 6 hr from 19 June 2017 to 18 October 2017 with a spatial resolution of 10 cm and strain resolution of 1.87 με. The measurements provided a clear-cut vertical profile of the strain changes caused by rainfalls that cannot be detected by conventional methods. The results show that there are two types of deformation in the landslide mass: (1) sliding at the boundary between tuff and mudstone and (2) creep in mudstone layers. Activation of deeper sections of the landslide by heavy rainfalls has also been detected.

Plain Language Summary This paper reveals in great detail the deformation process of a landslide corresponding to rainfall, which has never been detected in previous research, through the monitoring of the vertical distribution of strain changes with distributed fiber optic sensing analyzing Rayleigh backscattering. The measurements were completed on 18 October 2017. Therefore, this paper needs to rapidly report the results. This paper visualizes the unknown deformation of a mudstone layer below a slip plane that has been gradually activated by heavy rainfalls. The detection of the deformation of deeper zones leading to a larger landslide is a significant advance in disaster prevention and mitigation. The applicability of this technique to strain measurements for landslides shown in this paper suggests possible strain measurements for rocks in many research fields, including in studies of the deformations of active faults and volcanos.
The results shown in this paper may also be useful for researchers working in optics, photonics, and physical as well as geophysical research fields where they are trying to develop new technologies.

1. Introduction

A landslide is a form of mass wasting that includes a wide range of ground movements. Once deformation of a landslide is detected in its early stage, investigations are conducted to estimate the scale of the landslide or to predict larger deformations that would lead to a disaster. Vertical boreholes set in the landslide mass are frequently used for these investigations, into which sensors such as strain gauges or inclinometers are installed. These conventional sensors have been used at many landslide sites to measure strain or monitor landslide deformation.

Despite their popularity, however, the lower spatial resolutions of these sensors often make the measurands difficult to understand. These sensors are usually used to determine the depth/location of a slip surface, that is, the part that bends most. Therefore, more measurement points per unit length are preferable for accurate monitoring. The actual spatial resolutions for the sensors, however, are approximately 50 cm at minimum. Such low sensor spatial resolutions are highly related to the electrical supplies to the sensors. They work as discrete sensors using electricity provided from outside, and each sensor therefore has a pair of electrical wires. The number of electrical wires increases proportionally with the number of sensors, which causes congestion of wires in boreholes. Therefore, considering borehole depth and number of sensors, optimal spatial resolution becomes 50–100 cm in many cases. Consequently, the spatial resolutions of these sensors are sometimes insufficient to detect slight signs of deformation.

Fiber optic sensing is recognized as a promising method for measuring strain changes. Two major types of fiber optic sensing are available: fiber Bragg grating (FBG) and distributed fiber optic sensing (DFOS). A FBG is a type of distributed Bragg reflector constructed in a short segment of optical fiber that reflects

particular wavelengths of light and transmits all others. A FBG is a discrete point sensor that is similar to a strain gauge, although its strain resolution is much higher than that for strain gauges. Therefore, the increased spatial resolutions of FBGs also accrue greater costs and preparation times. Different from FBGs, one of the advantages of DFOS is that it can extract the measurand values (such as temperature, strain, pressure, corrosion, and vibration) as a function of the position along the entire length of the sensing fiber (Schenato, 2017). Therefore, DFOS can potentially replace a large number of discrete sensors (e.g., Soga et al., 2018).

Most DFOS studies have analyzed Brillouin backscattering. Among various fiber optic-based distributed sensing technologies, time domain techniques called Brillouin optical time domain reflectometry or analysis (BOTDR or BOTDA) are frequently used to measure strain changes. Another technique for DFOS that was first proposed in 1980 is based on Rayleigh backscattered light (Rogers, 1980). The number of publications on Rayleigh-based DFOS per year has continued to increase (Palmieri & Schenato, 2013). Coherent optical time domain reflectometry (COTDR), which is a Rayleigh-based DFOS technique, has higher resolution for measuring strain and temperature than Brillouin-based DFOS (Koyamada et al., 2006, 2009). DFOS with COTDR has been recently applied to strain measurements in laboratory tests (Kogure et al., 2015) and field measurements (Xue et al., 2014; Xue & Hashimoto, 2017), but only a few studies have demonstrated the effectiveness of this technique in Earth science research fields.

DFOS has also been introduced to the monitoring of landslide motion. Schenato et al. (2017) developed an experimental physical model and showed a planar strain distribution with artificial rain by analyzing Rayleigh scattering. For field measurements, Zeni et al. (2015) installed inclinometers based on Brillouin scattering into a borehole to detect strain changes of slow soil movements. The extensive measurement range of DFOS, higher strain resolution provided by COTDR, and simplicity of the installation of wireless fiber optic cables will make it a popular technique in this research field in the immediate future. Here we evaluate the effectiveness of strain measurements in an actual landslide using DFOS with COTDR. This paper reports the results of field-scale measurements of strain changes in the landslide and shows a vertical profile that extended from the ground surface to the bottom of the borehole.

2. Studied Landslide

A fiber optic cable was installed in a landslide located in Izumo, Shimane, Japan. Figure 1 shows a plan view and a cross section of the landslide, and its width and length are approximately 30 and 60 m, respectively. The bedrock around the landslide is rhyolite from the Miocene, and it is covered with mudstone and tuff. The upper layer of the mudstone and tuff is composed of talus deposits (ground surface). The thickness of the talus deposits varies with the location (Figure 1b). The layers form a dip slope.

The landslide occurred 20 years ago. The Shimane local government had already conducted investigations on the landslide prior to this study. The general water levels in boreholes BP1 and BP2 (Figure 1a) were approximately 10 and 5 m below ground level (BGL), respectively (Figure 1b). The water level increases by 1–5 m during rainfalls, which leads to strain changes in the boreholes. These changes in water level and strain were measured by water level gauges and inclinometers in the same boreholes. The strain changes were detected at a depth of 8 m for BP1 and 6.5 m for BP2; these depths represent the boundary between tuff and mudstone in BP1 (supporting information Figure S1a) and a highly weathered zone in the tuff in BP2 (Figure S1b). Consequently, the depth of the slip plane in this landslide was estimated at 6–8 m BGL based on these investigations (Figure 1b). The local government had also completed certain countermeasures such as steel pipe piles, drainage boring, and infiltration wells. Therefore, the landslide mass appears to be stable because of the countermeasures.

3. Principle of DFOS With COTDR

A benefit of DFOS compared to a strain gauge or inclinometer is that it is free from electrical noise due to the lack of electricity inside a cable (e.g., Soga et al., 2018). Therefore, DFOS is especially suitable for long-term or long-distance measurements that are susceptible to electrical disturbances. DFOS works as a strain sensor and is similar to a strain gauge rather than an inclinometer. DFOS and strain gauges measure differences in strain, whereas inclinometers literally measure changes in slope inclination, which results in the estimation of actual deformation.

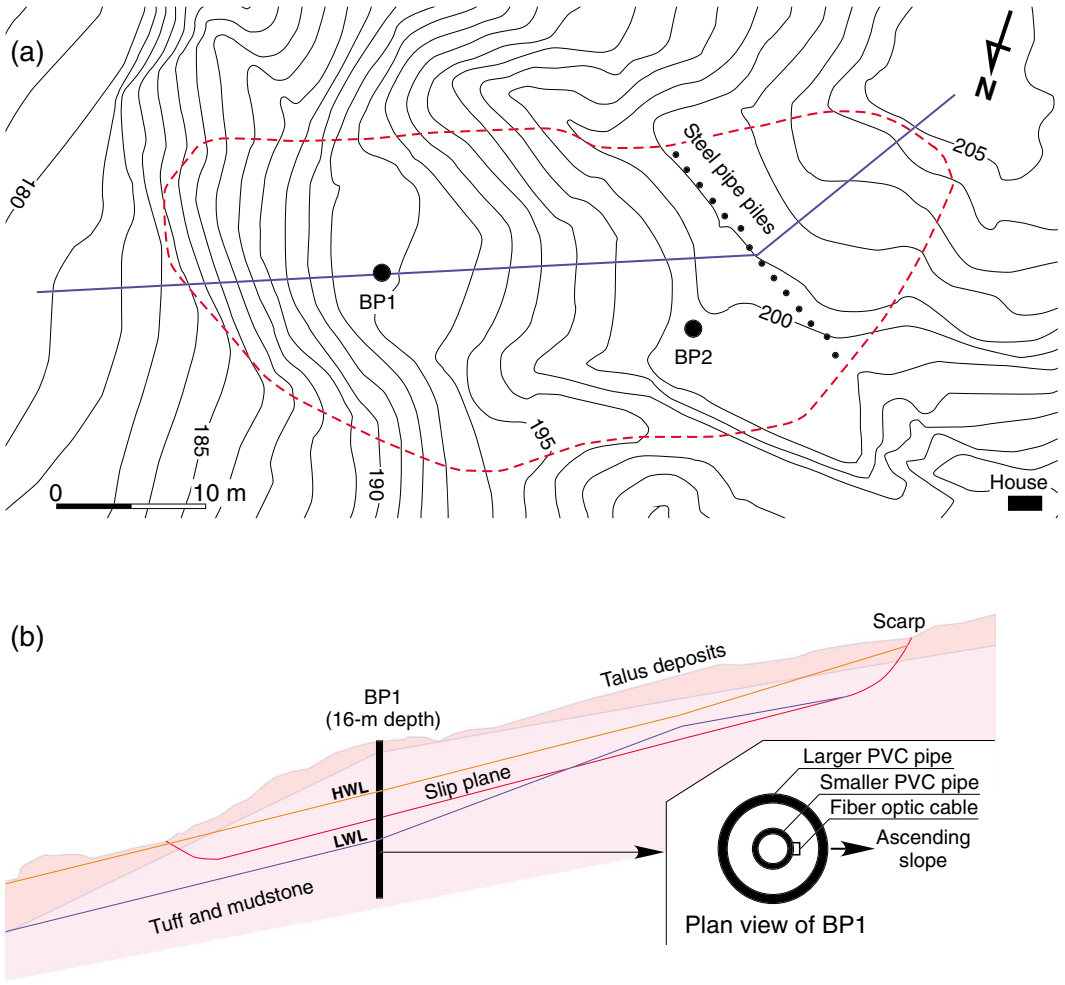

Figure 1. Geological setting of the investigated landslide: (a) plan view and (b) cross section along the blue line in Figure 1a. HWL = high water level; LWL = low water level. This information was provided by the Shimane local government.

The random distribution of a power spectrum in the COTDR trace in Rayleigh backscattering is inherent because of the heterogeneity of the glass density in the fiber core. The power spectrum shifts with environmental changes, such as temperature or strain. After the environmental changes, the previous power spectrum is restored by injecting light with a frequency different from that of the previous incident light. This technique is called tunable wavelength COTDR (TW-COTDR, Kishida et al., 2014). The difference in frequency between the two incident light beams before and after the environmental changes is proportional to the change in temperature or strain. Hereafter, the term frequency shift denotes the spectrum correlation used to restore the previous power spectrum, although the frequency of Rayleigh backscattering does not actually vary with environmental changes. We emphasize that the measurements refer to an initial state, and therefore, they are not absolute measurements.

The frequency shift depends on both the strain and temperature variations during the measurements. Therefore, the effect of the variations in these parameters on the shift should be evaluated separately if they change simultaneously, such as during rainfalls. Schenato et al. (2017) placed a fiber optic cable independent from strain in their physical model experiments to compensate for the effects of temperature variations in the data as well as other cables to measure data on the changes in strain and temperature. Frequency shifts in Rayleigh backscattering, denoted as $\Delta\nu_R$, are expressed as follows (Kishida et al., 2014):

$$\Delta\nu_R = \alpha\Delta\varepsilon + \beta\Delta T, \tag{1}$$

where $\Delta\varepsilon$ and ΔT denote the changes in strain and temperature, respectively, and α and β (corresponding to C_{21} and C_{22} in Kishida et al., 2014) denote the sensitivity coefficients for strain and temperature, respectively.

The coefficients are used to convert the frequency shift into the amount of strain and temperature change. The values of the coefficients for the cable used in this study (Fujikura Ltd., Tokyo, Japan, FR-OG4ETINHE-SR15E × 4C, which includes four single-mode fibers) were measured via laboratory tests prior to the installation of the cable in the landslide, and the values of α and β were -0.134 GHz/με and -3.36 GHz/°C, respectively. These values should be evaluated for each cable. In this study, the values were measured without removing the polyethylene sheath from the cable, which is the same condition for the strain measurements of the landslide, including the effect of thermal expansion of cover material.

4. Fiber Optic Cable Installation and Measurement Settings

Rayleigh backscattering was analyzed using a NBX-7020 (Neubrex Co., Ltd., Kobe, Japan). The instrument was set in a house near the landslide (Figure 1a). The fiber optic cable ran from the instrument to the landslide mass and was then turned up at the bottom of BP1 before returning to the instrument in the house. The whole length of the cable was approximately 460 m. The cable was directly buried at a depth of 30 cm BGL except for inside BP1. The cable was attached to the surface of a pipe made of polyvinyl chloride (PVC) with plastic tape so as not to slip at the boundary between the cable and pipe and vertically set into a larger PVC pipe equipped in BP1. Tensile stress was applied to the cable to provide pretensioning at that moment. The lengths of the smaller and larger PVC pipes were both 16 m, and the inner (outer) diameters of the smaller and larger PVC pipes were 13 mm (18 mm) and 40 mm (48 mm), respectively. The larger pipe was coupled with BP1 by filling the annulus with grout. The smaller pipe with fiber optic cable was also fixed inside the larger pipe by grouting, with the cable facing an ascending slope (Figure 1b). Therefore, in this case, positive and negative strain indicates the deformation of the pipes to the descending and ascending slope, respectively. Similar to a measurement principle in strain gauges (e.g., Ochiai et al., 2004), a negative strain indicates shrinking of the previously extended cable caused by bending of the smaller pipe toward the ascending slope. The tops of the pipes were covered with a PVC cap, and the inside of the smaller pipe remained hollow.

Strain measurements started in 19 June 2017 after the acquisition of initial frequency used as a reference, which was 2 weeks after the grouting to avoid possible effects of rapid changes in temperature on the analysis for Rayleigh backscattering. The spatial resolution of the strain measurements was set to 10 cm. The strain resolution was 1.87 με, which corresponded to a temperature resolution of 0.074 °C. Each measurement required approximately 45 min of processing under the current measurement settings. The processing time varied with different measurement settings such as the entire length of cable, spatial resolution, and strain resolution. The time interval of the measurement was fixed at 6 hr.

The frequency shift should be separated into shifts caused by changes in strain and changes in temperature. Schenato et al. (2017) reported that temperature compensation caused by rainfall had a limited effect on the spectral shift because of slope-induced strain. They measured temperature change at 60 cm BGL in permeable loose soil (sand), and the value was negligible; therefore, the effect of temperature change caused by rainfall can also be considered negligible in this study. The effect of air temperature changes on frequency shifts should also be considered. Hall et al. (2012) reported the influence of the thermophysical properties of pavement materials on the evolution of temperature depth profiles in different climatic regions. They showed that heated pavement caused changes in soil temperature from 0 to 1 m BGL, and changes deeper than 1 m were not observed. Furthermore, most of the studies discussing seasonal changes in ground temperature in cold regions considered the near-surface zone shallower than 1 or 2 m (e.g., Hirota et al., 2002). On the other hand, it is commonly understood in geothermal energy research that annual soil temperature fluctuates up to 10 m BGL because of ground heat supplied by the sun and rain, although it varies with soil composition and other environmental conditions (Márquez et al., 2016). On average, the underground temperature at 10 m BGL remains constant throughout the year and is substantially equal to the average temperature of the place (Buzăianu et al., 2015; Graf et al., 2016). Based on these studies, we considered that the long-term temperature changes up to 10 m BGL might affect frequency shift in this study rather than short-term changes caused by temporal rainfall or sunlight (the thermal conductivities and volumetric heat capacities of rocks related to ground thermal diffusivity do not allow sharp changes in deeper rock/soil temperatures). However, considering that frequency shifts caused by landslide deformation and long-term temperature changes will occur at different time scales (shorter for landslides and longer for temperature

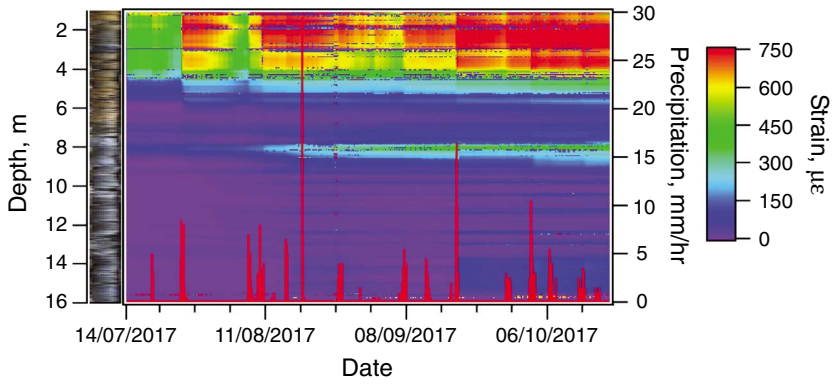

Figure 2. Color map showing the strain changes along borehole BP1 from 14 July 2017 to 18 October 2017 as well as a rock-core image and precipitation information.

changes) and that frequency shifts by landslides predicted by previous studies were much larger than those due to temperature changes, we expect that strain changes induced by rainfall will be successfully detected by DFOS, although values of strain difference might be slightly overestimated. Therefore, we discuss strain changes from 1 to 16 m BGL using equation (1). After substituting the sensitivity coefficient for strain and frequency shift into equation (1), without including the member related to temperature, the equation can be solved to determine the changes in strain. Here we again emphasize that strain difference can be overestimated because of the effect of temperature change, which will be discussed in the next section.

5. Strain Changes at Different Depths

Figure 2 shows a color map of the distribution of strain changes along BP1 calculated by equation (1), which might have included the effect of temperature change as mentioned above. The color map shows the results from 19 June 2017 and a specific time. A picture of a core that was previously drilled from BP1 by the local government is presented at the left-hand side of the color map. The vertical scale is equivalent between the color map and the picture, that is, from 1 m to 16 m BGL. The vertical bars on the lateral axis of the color map show the hourly rainfall recorded at a weather station of the Japan Meteorological Agency located 20 km away from the landslide.

Sharp changes in color in the vertical direction, especially at the near-surface zone, indicate that the effect of air temperature changes on frequency shifts is smaller compared with the effect of strain changes. If the air temperature change had a stronger effect on the frequency shift relative to the strain change, the map would show gradual changes in color from the top to the bottom. Furthermore, our measurements show abrupt increases in strain accompanied by rainfalls, and the strain changes are of the same order as measured in a physical model experiment with artificial rainfall by Brillouin optical time domain analysis (Yan et al., 2017) and in shallow landslides with inclinometers and strain gauges (Nakai et al., 2016; Sonoda & Kurashige, 2017). Several hundred micro strain of strain changes have been detected in this study, although the strain changes in the near-surface zone (1–4 m BGL) could be overestimated by 125–175 με due to possible temperature changes (Figures 2, S2, and S3). Based on these studies and discussions, we recognize that DFOS appears to successfully measure rainfall-induced strain changes, which is the purpose of this study, although it might include overestimations, especially in the near-surface zone. The discussions below are based on this recognition.

Horizontal dots in lines shown in cold colors represent measurement noise related to grouting for the cable, and this noise was more obvious at specific depths at which large strain changes were measured. The deformation of BP1 can lead to decoupling between the cable and grout, which results in noise. Grouting materials with low elasticity may reduce the noise. However, local strain changes over the whole range of BP1 could be observed using the map despite the noise.

Figure 2 shows that the strain varies with time and depth and provides insights regarding the deformation of the landslide. Distinctive strain changes are found at the depths of (1) 1–5 m, (2) approximately 8 m, and (3)

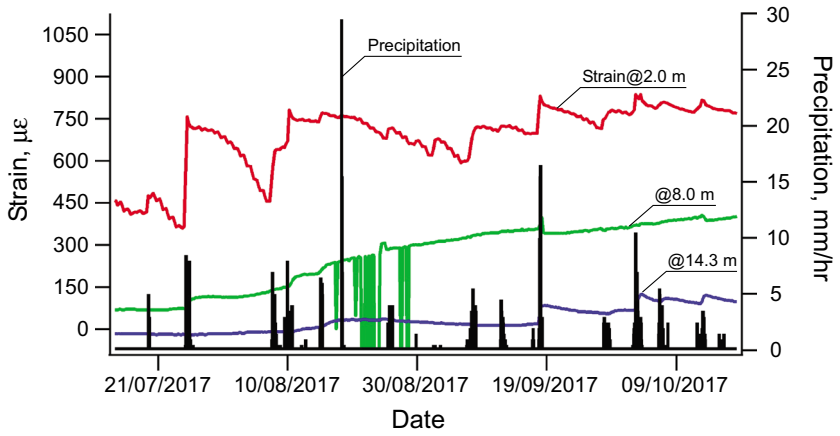

Figure 3. Strain changes at 2.0, 8.0, and 14.3 m together with the precipitation levels. Fluctuations at 8.0 m appear to be noise.

14–15.5 m. The strain changes around 8 m appear to show a deformation of the slip plane because the depth is coincident with that previously recognized as the slip plane by the local government. Figure 2 reveals that the slip plane, which is presented as a sharp contrast in color and corresponds to the boundary between tuff and mudstone layers, is actually located at 8 m (Figure S1a). The thickness of the deformation zone across the slip plane slightly increases over time. The upward and downward propagation of the strain changes across the slip plane appear to indicate that the range of BP1 bending across the slip plane broadens as the landslide approaches the descending slope.

The largest strain changes appear near the ground surface, which is mainly composed of mudstone. The strain distribution in the vertical direction implies that this section can be divided into sections with different strain changes. The DFOS used in this study detects such small differences in the strain changes, which may be produced by discontinuous planes or differences in the physical and mechanical properties. Abrupt strain changes along the horizontal axis, shown as rapid changes in color, are also detected in this section. In particular, abrupt increases in strain occur on the same date as rainfall events, and the strain then gradually decreases after the rainfall. A similar trend of strain changes is also found below the slip plane at 14–15.5 m BGL, which is included in the mudstone layer, although the values are smaller than those in the uppermost section.

6. Sensitivity of Strain Change to Rainfall

Figure 3 shows the time variations in precipitation and strain changes at the depths of 2, 8, and 14.3 m, which are representative of the uppermost section, the slip plane, and the bottom section, respectively. This figure indicates that the strain changes at 2 m are nearly consistent with the occurrence of rainfalls except for the most extreme precipitation event (29.5 mm/hr) in the middle of August. This extreme event was confirmed to be a localized rainfall event around the Japan Meteorological Agency weather station induced by an intense but small nimbus. The strain largely increased because of rainfall and then gradually decreased toward the previous level until the next events occurred in July and early August. A similar fluctuation in strain changes before and after rainfall has also been reported via a strain measurement recorded using inclinometers or strain gauges for a shallow landslide (e.g., Nakai et al., 2016; Sonoda & Kurashige, 2017). Nakai et al. (2016) explained that shearing occurred during rainfalls and that the decreasing strain was caused by the soil drying process. The consistency in the trend of strain changes in Nakai et al. (2016) and Sonoda and Kurashige (2017) and in the present study also suggests that the long-term temperature change does not disturb the measurements of rainfall-induced strain change.

The sensitivity of the strain change to rainfall appears to decrease after precipitation events related to Typhoon Noru and a front from 7–10 August, with a total precipitation of 65.5 mm. After these events, the variation in strain changes presents lower fluctuations before converging. However, the strain changes at 14.3 m become obviously sensitive after 17 September when the daily precipitation reached 78 mm,

although the changes are not related to the precipitation prior to the heavy rain. After the event, the strain changes at 14.3 m also present rapid increases corresponding to rainfall events and then gradually decrease, which is similar to the trend at 2 m. Moreover, the strain changes at 2 and 14.3 m both occur in mudstone and appear to start synchronizing after the rainfall event. However, the strain changes at 8 m are slightly different from those at other depths. Rapid increases in strain at this depth (but slower than those at 2 m) are induced by rainfall until the middle of the August, and then the strain changes become less sensitive to rainfall, which is also observed at 2 m. However, even if the rain stops, the strain continues to increase until the end of the measurement duration, and the strain changes are not related to rainfall after the middle of August.

7. Different Deformation Process in the Landslide Mass

The deformation process of the slip plane must be different from that at 2 and 14.3 m as mentioned above. The different thicknesses of the deformation zones at the three studied depths also appear to be caused by different deformation processes. The uppermost section (1–5 m BGL) shows almost constant strain changes over the entire thickness, which is similar to that in the bottom section (14–15.5 m BGL). Namely, the thickness in these sections is larger than that in the slip plane (Figure 2). The larger thickness of the deformation zone and fluctuation in the strain changes suggest that the deformation process in these sections is not a slip but a creep (Selby, 1993; Sonoda & Kurashige, 2017). For the uppermost section, based on our results and the interpretation by Nakai et al. (2016), the fluctuation in strain changes can be interpreted as follows: (1) the increased weight of the rock caused by an increase in water saturation by rainfall deforms the section toward the descending slope, which leads to an increase in strain; (2) the strain decreases as the water saturation decreases, meaning that the weight of the rock reduces via drying or drainage after the rainfall until the next rainfall; and (3) repetitive fluctuations cause the section to become more solid and thus less sensitive to rainfall. Alternatively, the deformation process may have been changed in the bottom section because fluctuations similar to that in the uppermost section do not occur until 17 September. The bottom section appears to be gradually activated by certain rainfall events with high precipitation levels as mentioned above. The delay in the commencement of the strain changes in the bottom section indicates that the depths of the active sections propagate from upper to lower as rainwater or ground water permeates into the deeper sections of the landslide, thereby increasing pore pressure after 17 September. Therefore, this result suggests that a water permeation process inside the landslide changes with the amount of precipitation. The combination of DFOS and water level investigations will provide further insights into this process.

8. Concluding Remarks

Importantly, our measurements revealed the deformation of the lower section of the landslide under the slip plane composed of mudstone despite the small strain changes. The conventional view of landslides in which rocks below a slip plane are fixed, stable, and impermeable for a long time may need to be modified when conducting simulations or experiments using a physical model. Our data clearly show the deformation of the bottom section after heavy rainfalls, which implies water permeation deep into the mudstone. Disaster prevention and mitigation efforts should focus on such significant deformations because they could induce a larger landslide. Large strain changes in other sections in addition to those in the slip plane have also been detected. The deformations of the upper and bottom sections of the landslide were unknown until this study because they were not detected during investigations conducted by the local government using conventional methods.

The spatial and strain resolution of DFOS with TW-COTDR cannot be achieved with most conventional methods, and these parameters enabled us to develop a comprehensive image of the distribution of strain changes. These resolutions appear to be sufficiently high to realize the distribution of strain changes for landslide monitoring. In addition to landslides, this method can be applied to monitor rock deformations in many fields, such as scientific research studies or geoengineering studies, via the measurements of strain changes. For example, the monitoring of strain changes across an active fault using this technique will provide insightful measurand values to enable a better understanding of the occurrence of earthquakes related to strain accumulation.

In summary, this study demonstrated that DFOS with COTDR is a promising geophysical exploration method. The results showed that the method produces a clear-cut vertical profile of strain changes along a borehole,

even in a landslide for which countermeasures had been implemented. The applicability of DFOS with COTDR to perform measurements of strain changes (as demonstrated in this study) will facilitate the replacement of a large number of discrete sensors with DFOS. The correction of possible overestimations of strain changes caused by temperature changes remains to be addressed in order to increase measurement accuracy.

Acknowledgments
The authors are grateful to the local government of Shimane for providing data from their investigations of the landslide. We would also like to thank Neubrex Co., Ltd. for analyzing the frequency shift and providing suggestions on DFOS. This study was supported partly by JSPS (grant 15H05350) to T. K. This manuscript has been improved by comments and suggestions from Cardenas and two anonymous reviewers. Data to support this research are available from the following link: 10.6084/m9.figshare.6080549.

References

Buzăianu, A., Csáki, I., Moţoiu, P., Popescu, G., Thorbjornsson, I., Ragnarsodottir, K. R., et al. (2015). Recent advances of the basic concepts in geothermal turbines of low and high enthalpy. *Advances in Materials Research*, *1114*, 233–238. https://doi.org/10.4028/www.scientific.net/AMR.1114.233

Graf, S., Lanzerath, F., Sapienza, A., Frazzica, A., Freni, A., & Bardow, A. (2016). Prediction of SCP and COP for adsorption heat pumps and chillers by combining the large-temperature-jump method and dynamic modeling. *Applied Thermal Engineering*, *98*, 900–909. https://doi.org/10.1016/j.applthermaleng.2015.12.002

Hall, M. R., Dehdezi, P. K., Dawson, A. R., Grenfell, J., & Isola, R. (2012). Influence of the thermophysical properties of pavement materials on the evolution of temperature depth profiles in different climatic regions. *Journal of Materials in Civil Engineering*, *24*(1), 32–47. https://doi.org/10.1061/(ASCE)MT.1943-5533.0000357

Hirota, T., Pomeroy, J. W., Granger, R. J., & Maule, C. P. (2002). An extension of the force-restore method to estimating soil temperature at depth and evaluation for frozen soils under snow. *Journal of Geophysical Research*, *107*(D24), 4767. https://doi.org/10.1029/2001JD001280

Kishida, K., Yamauchi, Y., & Guzik, A. (2014). Study of optical fibers strain-temperature sensitivities using hybrid Brillouin-Rayleigh system. *Photonic Sensors*, *4*(1), 1–11. https://doi.org/10.1007/s13320-013-0136-1

Kogure, T., Horiuchi, Y., Kiyama, T., Nishizawa, O., Xue, Z., & Matsuoka, T. (2015). Fiber optic strain measurements using distributed sensor system under static pressure conditions (in Japanese with English abstract). *BUTSURI-TANSA*, *68*(1), 23–38. https://doi.org/10.3124/segj.68.23

Koyamada, Y., Eda, Y., Hirose, S., Nakamuka, S., & Hogari, K. (2006). Novel fiber-optic distributed strain and temperature sensor with very high resolution. *IEICE Transactions on Communications*, *E89-B*, 1722–1725. https://doi.org/10.1093/ietcom/e89-b.5.1722

Koyamada, Y., Imahama, M., Kubota, K., & Hogari, K. (2009). Fiber-optic distributed strain and temperature sensing with very high measurand resolution over long range using coherent OTDR. *Journal of Lightwave Technology*, *27*(9), 1142–1146. https://doi.org/10.1109/JLT.2008.928957

Márquez, J. M. A., Bohórquez, M. Á. M., & Melgar, S. G. (2016). Ground thermal diffusivity calculation by direct soil temperature measurement. Application to very low enthalpy geothermal energy systems. *Sensors*, *16*, 306. https://doi.org/10.3390/s16030306

Nakai, S., Watanabe, S., Sasahara, K., & Iwata, N. (2016). Relationship between shear deformation and soil moisture content due to rainfall in a surface soil of granite slope (in Japanese with English abstract). *Japan Geotechnical Journal*, *11*(2), 115–125. https://doi.org/10.3208/jgs.11.115

Ochiai, H., Okada, Y., Furuya, G., Okura, Y., Matsui, T., Sammori, T., et al. (2004). A fluidized landslide on a natural slope by artificial rainfall. *Landslides*, *1*(3), 211–219. https://doi.org/10.1007/s10346-004-0030-4

Palmieri, L., & Schenato, L. (2013). Distributed optical fiber sensing based on Rayleigh scattering. *Open Optical Journal*, *7*(1), 104–127. https://doi.org/10.2174/1874328501307010104

Rogers, A. J. (1980). Polarisation optical time domain reflectometry. *Electronics Letters*, *16*(13), 489–490. https://doi.org/10.1049/el:19800341

Schenato, L. (2017). A review of distributed fibre optic sensors for geo-hydrological applications. *Applied Sciences*, *7*(9), 896. https://doi.org/10.3390/app7090896

Schenato, L., Palmieri, L., Camporese, M., Bersan, S., Cola, S., Pasuto, A., et al. (2017). Distributed optical fibre sensing for early detection of shallow landslides triggering. *Scientific Reports*, *7*(1), 14686. https://doi.org/10.1038/s41598-017-12610-1

Selby, M. J. (1993). *Hillslope materials and processes*. Oxford, UK: Oxford University Press.

Soga, K., Kechavarzi, C., Pelecanos, L., de Battista, N., Williamson, M., Gue, C. Y., et al. (2018). Fiber-optic underground sensor networks. In S. Pamukcu & L. Cheng (Eds.), *Underground sensing* (pp. 287–356). Cambridge, Academic Press. https://doi.org/10.1016/B978-0-12-803139-1.00006-0

Sonoda, M., & Kurashige, Y. (2017). Characteristics of surface soil creep on a forest slope in Japan. *Geomorphology*, *288*, 1–11. https://doi.org/10.1016/j.geomorph.2017.03.006

Xue, Z., & Hashimoto, T. (2017). Geomechanical monitoring of caprock and wellbore integrity using fiber optic cable: Strain measurement from the fluid injection and extraction field tests. *Energy Procedia*, *114*, 3305–3311. https://doi.org/10.1016/j.egypro.2017.03.1462

Xue, Z., Park, H., Kiyama, T., Hashimoto, T., Nishizawa, O., & Kogure, T. (2014). Effects of hydrostatic pressure on strain measurement with distributed optical fiber sensing system. *Energy Procedia*, *63*, 4003–4009. https://doi.org/10.1016/j.egypro.2014.11.430

Yan, J., Shi, B., Ansari, F., Zhu, H., Song, Z., & Nazarian, E. (2017). Analysis of the strain process of soil slope model during infiltration using BOTDA. *Bulletin of Engineering Geology and the Environment*, *76*(3), 947–959. https://doi.org/10.1007/s10064-016-0916-0

Zeni, L., Picarelli, L., Avolio, B., Coscetta, A., Papa, R., Zeni, G., et al. (2015). Brillouin optical time-domain analysis for geotechnical monitoring. *Journal of Rock Mechanics and Geotechnical Engineering*, *7*(4), 458–462. https://doi.org/10.1016/j.jrmge.2015.01.008